Biorheology 43 (2006) 147–159
IOS Press

Geometrical focusing of cells in a microfluidic device: An approach to separate blood plasma

Magalie Faivre, Manouk Abkarian, Kimberly Bickraj and Howard A. Stone *
Division of Engineering and Applied Sciences, Harvard University, Cambridge, MA 02138, USA

Received 30 September 2005
Accepted in revised form 12 January 2006

Abstract. It is well known that when a suspension of cells flows in small vessels (arterioles or venules), there exists a cell-free layer of a few microns adjacent to the vascular walls. Using an *in vitro* model, we show experimentally that for a fixed flow rate a geometrical constriction in the flow can artificially enhance the cell-free layer. Also, we show that rapid variation of the geometry coupled to the deformability of the cells can dramatically modify their spatial distribution in the channel. The effects of the constriction geometry, flow rate, suspending fluid viscosity, cell concentration, and cell deformability are studied and the results are interpreted in terms of a model of the hydrodynamic drift of an ellipsoidal cell in a shear flow. We propose a microfluidic application of this focusing effect for separation of the red blood cells from the suspending plasma.

Keywords: Lift force, cell-free layer, red blood cells, hemodilution

1. Introduction

Blood plasma transports, among other products, the gases of respiration (O_2, CO_2) *via* the red blood cells, the metabolic wastes of the cells (urea), the molecules that play a fundamental role in defense (anti-bodies), the cells of the immune defense (leukocytes and lymphocytes), the products of digestion (glucose, lipids, amino acids and ions), the diverse internal (enzymes and hormones) and external (vitamins) biocatalysts, and the molecules of coagulation (fibrinogen). Hence, analyses of the plasma are used intensively in clinical hematology to study infections and diseases [25]. Nevertheless, to characterize the plasma content it is essential to separate it from the cells without depleting the molecular constituents. Traditionally, this separation is done through centrifugation. An alternative strategy to produce separation of plasma and blood cells is to use the natural tendency of sheared deformable cells to move away from boundaries, i.e. drift *via* hydrodynamic lift [9,10,12]. In this paper, we show how a rapid variation of the cross-section of a microfluidic channel modifies the spatial distribution of cells downstream of a constriction and increases the cell-free layer adjacent to the boundary. We quantify different aspects of this geometrical enhancement and use this understanding to demonstrate an approach

*Address for correspondence: Dr. H.A. Stone, Division of Engineering and Applied Sciences, Harvard University, Cambridge, MA 02138, USA. Tel.: +1 617 495 3599; Fax: +1 617 495 9837; E-mail: has@deas.harvard.edu.

to extract continuously and simultaneously a stream of pure plasma and a concentrated stream of blood cells.

Indeed, one of the topical challenges in biochemistry and biomedicine is to develop continuous and inexpensive tools for handling small volumes of blood to study simultaneously and separately the blood cells and their suspending plasma. During the last decade, microfluidic approaches have led to many developments toward a "lab-on-a-chip" [2]. The basic idea is to miniaturize (typically the channels have dimensions tens of microns) and make continuous large-scale laboratory tasks, which thus dramatically reduces the cost and volume of fluid used. The approach introduced for separation in this paper can be readily integrated into existing lab-on-a-chip microdevices [22,23].

At the heart of our investigation lies the concept of hydrodynamic lift of deformable cells in shear flow and the cell-free layer produced adjacent to the boundaries. These ideas are commonly discussed in the hemodynamics literature. Indeed, one of the oldest and best known hemodynamic phenomenon of the microcirculation is the Fåhraeus effect [11,19], which refers to the decreased hematocrit concentration in small tubes relative to the larger reservoirs to which they are connected [1]. The Fåhraeus effect is well understood as arising from hydrodynamic drift of the deformable cells away from the high shear rate (and high shear stress) regions adjacent to the walls of the vessel [8,10,12]. Thus, a cell-free layer, typically comparable to the size of a single cell, exists in large portions of the microcirculation. This cell-free layer is also responsible for the nonuniform distribution of cells in a vessel network such as a tissue. Briefly, the concentration of red blood cells in a network of daughter arterioles, capillaries or venules in the microcirculation can be lower than the concentration in the mother feeding vessel; this is usually referred to as the plasma skimming or the network Fåhraeus effect [11,19]. As we show below, we used the plasma skimming concept as a developmental strategy to design a microdevice for separation of cells from plasma.

In this article we investigate the flow of healthy and modified red blood cells in micron-size channels containing a constriction. Direct visualization is used to measure the distribution of cells up- and downstream of the constriction. We document the effect of the different parameters of the system, including geometry of the constriction (e.g. its length and width), flow rate, viscosity of the suspending media, cell concentration, and deformability of the cells. We also provide a model for the change in the distribution of the cells that incorporates the major geometrical and dynamical variables and explains qualitatively (and in some cases quantitatively) the effect of a constriction on the downstream cell distribution for variations of all of the parameters studied. Finally, we show how these ideas can be integrated into the design of a microfluidic component for continuous separation of blood cells and plasma.

2. Materials and methods

2.1. Device fabrication

The microfluidic experiments used relief molds that were produced using common soft-lithography techniques [6]. The channels were made of poly(dimethylsiloxane) (PDMS) and bonded to a glass microslide by surface plasma treatment in air. An illustration of the apparatus is shown in Fig. 1a. The channel height was measured by a profilometer to be 75 μm everywhere (even at the constriction) and the channel width was 100 μm. The lengths L of the symmetrical rectangular constrictions (Fig. 1b) were varied from 50 to 300 microns and the widths w from 15 to 50 microns.

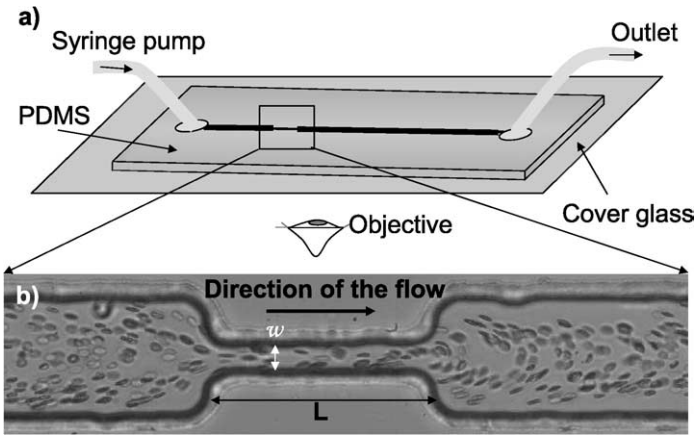

Fig. 1. Microfluidic setup for the flow of red blood cells through a constriction. The channel height is 75 μm and the dimensions of the constriction shown are $L = 200$ μm and $w = 25$ μm. (a) Side view. (b) Top view.

2.2. Solutions

The blood used in all of the experiments was collected from a single healthy donor. In order to prevent their aggregation over long times and their adhesion on the non-treated channel walls, we washed the cells twice in a solution of Phosphate Buffer Saline (PBS), which had an osmotic pressure of 300 ± 10 mOsmol/kg and a pH of 7.4. After gentle centrifugation, this model cellular solution was dispersed into the suspending media chosen for the experiment. For most of the experiments, two concentrations of red blood cells were studied: 0.1% v/v and 2.6% v/v hematocrit; in the last experimental demonstration given in the paper, we use 16% hematocrit. We note that the typical volume of a normal cell at 300 mOsmol is about 94 μm^3 [7].

In order to test the effect of the viscosity of the surrounding fluid, two suspending media were prepared by dissolving dextran (molecular weight equal to 2×10^6) in the PBS buffer. The viscosities of the solutions were measured to be 0.02 Pa.s and 0.047 Pa.s, respectively, at concentrations of 6% and 9% w/w dextran. Although dextran is known to facilitate aggregation of blood cells, no aggregates were observed during the time of our experiments. The use of the high-speed camera allows us to verify that each RBC passing through the constriction was not attached to, or aggregated with, its neighbors.

The rigidity of the red blood cells was modified using a standard method [5]. First, the cells were treated with a solution of glutaraldehyde 1% v/v while being agitated for ten minutes. Then, the cells were washed again in PBS (as explained previously) and dispersed in a solution of dextran with a viscosity of 0.02 Pa.s. After the treatment with glutaraldehyde the cells are rigid with a fixed ellipsoidal shape.

We also modified the volume of the cells by changing the osmotic pressure of the surrounding fluid through the dilution of the PBS buffer previously prepared. The new osmotic pressure was measured to be 200 ± 10 mOsmol/kg. The modified buffer was used to wash the red blood cells and the cellular solution was dispersed in a solution of dextran with a viscosity of 0.02 Pa.s made with the hypotonic buffer. Such hypotonic conditions swell the cells, which have a new volume typically 116 μm^3 [7].

As a control we also studied trajectories of polystyrene beads, 8.7 microns in diameter, dispersed in a solution of dextran at a viscosity of 0.02 Pa.s. This size particle was chosen since it is the same as the maximum diameter of the cells.

2.3. Experimental procedures

Experiments were performed in a microfluidic setup adapted for standard light microscopy. We used a classical inverted microscope in bright field (Leïca DM IRB) with a 20× magnification. The syringe containing the suspension of blood is connected to the input of the microfluidic channel. The fluid is delivered at a constant flow rate by a standard motor-driven pump. We varied the applied flow rate from 10–1000 μl/hr, which corresponds to an average fluid speed of 0.1–10 cm.s^{-1}. Movies were taken with a high-speed camera (Phantom V5, using a frame rate 2000–5000 frames per second).

2.4. Procedures for image analysis

Image analysis of the experiments with 2.6% hematocrit was performed with the software "Image J". This software projects an image along the axis perpendicular to the image plane of the movie in order to detect the statistical distribution of red blood cells at a given position along the channel. The projection of the average intensity is output such that each pixel stores the average intensity over all images in the movie stack at a corresponding pixel location [14]. Hence, a region where statistically a large number of red blood cells pass will appear darker than the background (see Fig. 3a). In the case of the experiments conducted with a low concentration of cells (hematocrit of 0.1%), this approach is inefficient for localizing the cell-free layer (not enough cells are passing). Therefore, we also measured the cell-free layers on a given movie by visually locating the red blood cells closest to the walls and measuring their distance to the walls up- and downstream. We applied this second method to some movies obtained at 2.6% hematocrit in order to verify the good agreement of the results obtained by the two different procedures.

3. Experimental results

In this section we present experimental observations of a narrow cell-free layer upstream of the constriction [13,15] and document how this cell-free layer is substantially enhanced downstream of the obstruction. We systematically investigate the enhancement of the width of the cell-free layers downstream of the constriction by varying the flow rate, the geometry, the concentration or hematocrit, the viscosity of the suspending fluid, and the mechanical properties of the cells. Finally, the experimental results are used to design a separator that takes advantage of this constriction-enhanced cell-free layer.

First, it is important to recognize the constraints associated with low-Reynolds-number flows [3] and to exhibit the flow profiles for rigid particles. In Fig. 2 we show the trajectories of the centers of mass of rigid spherical particles, which have a size comparable to red blood cells, for typical flow conditions where the Reynolds number (based on the channel height) is about 0.01; the Reynolds number is calculated as $\rho_{\text{out}}Q/(\eta_{\text{out}}H)$, where ρ_{out} and η_{out} are, respectively, the density and viscosity of the suspending phase, Q is the flow rate, and H is the channel height. The trajectories are fore-aft symmetric about the center of the constriction, as expected since such particles follow the fluid and the streamlines of the flow are fore-aft symmetric when the Reynolds number is less than one. Consequently, for the asymmetric trajectories of red blood cells that we show below for the same magnitude of Reynolds numbers, we conclude that the asymmetries and the corresponding enhanced cell-free layer are due to some combination of the deformability and non-spherical shape of the cells.

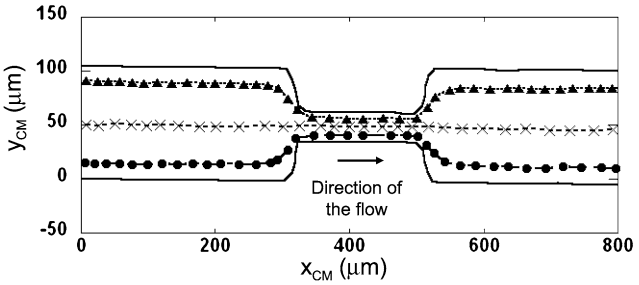

Fig. 2. Trajectories of three spherical polystyrene beads (8.7 microns in diameter) dispersed in a dextran solution with viscosity 0.02 Pa.s; $Q = 50$ μl/hr, $L = 200$ μm and $w = 25$ μm.

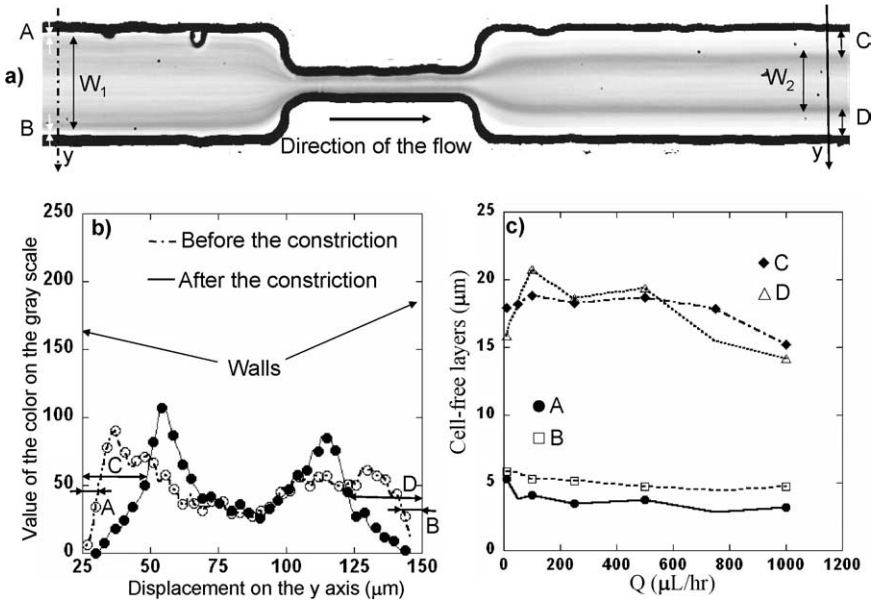

Fig. 3. (a) Image obtained after treatment of a typical movie by "Image J" software. A, B and C, D represent the cell-free layers, respectively, up- and downstream and W_1 and W_2 denote the widths of the distributions of the cells, respectively, before and after the constriction; $L = 200$ μm and $w = 25$ μm. (b) Value of the intensity of the gray scale versus the displacement y across the channel (○) before and (●) after the constriction. (c) Measured cell-free layers versus the flow rate Q with a hematocrit at 2.6%. The red blood cells are suspended in a dextran solution with viscosity 0.02 Pa.s; $L = 300$ μm and $w = 25$ μm.

3.1. Cell-free layers up- and downstream of the constriction

We begin with a description of the typical experiments with red blood cells in constricted flows (Fig. 3). In particular, there are regions of the flow that have essentially no cells, i.e. cell-free layers. We measure the locations and widths of the cell-free layers and we report also the widths of the distribution of cells before and after the constriction as shown in Fig. 3a. The gray-level image in Fig. 3a illustrates the existence of a cell-free layer, about 4 microns in width (which is half the size of a cell), before the constriction and clearly documents the substantial influence of the constriction on the downstream flow. A plot of the gray-scale values across the channel, both up- and downstream of the constriction, is shown in Fig. 3b. For the conditions in Fig. 3, the downstream cell-free layers have been enhanced to about 18

microns, which is roughly twice the size of the cell. We scanned more than 1 centimeter downstream of the constriction and, perhaps surprisingly, the enhanced cell-free layer remains largely unchanged.

The data also suggest one additional feature introduced by the constriction: assuming an approximate correspondence between the gray-scale level and the cell number density, we note in Fig. 3b that there appears to be a maximum cell density off the centerline and somewhat close to the wall. We shall return to this point below.

3.2. Enhancement of the downstream cell-free layer as a function of the different parameters

We next investigate the effect of the flow rate. In Fig. 3c, we report, as a function of the flow rate Q, the evolution of the cell-free layers at the top and bottom walls up- and downstream of the constriction, respectively labelled as A, B and C, D. We note in the Fig. 3c that the effect of the constriction is symmetrical top to bottom, as the cell-free layers near the upper and lower walls are equivalent (A $\approx$ B and C $\approx$ D). Upstream of the constriction the cell-free layers A and B are equal in width (on the order of 4 microns) and slightly decrease with the flow rate Q. The cell-free layers C and D decrease only a little as we increase Q and tend to the same value (about 15 microns).

We then extract the widths of distribution of the red blood cells up- and downstream, respectively denoted W_1 and W_2. A plot of the ratio W_2/W_1 versus the flow rate Q is shown in Fig. 4a for four different lengths of the constriction. Representative images of the different geometries are shown also. The results show very little variation of the cell-free regions with the flow rate, but the cell-free layer is enhanced significantly for larger lengths of the constriction.

It is clear that the constriction is responsible for enhancement of the cell-free layer so we now document the effect of the geometry of the constriction for a fixed viscosity of the outer fluid of 0.02 Pa.s. Because of the weak effect of Q on W_2/W_1, the mean values of W_2/W_1 (Fig. 4a) are extracted from the gray-level data and reported versus the length L of the constriction for a fixed width w or versus w for a fixed L. These results are shown in Fig. 4b. Although we do not have extensive data on the influence of the constriction width, it is nevertheless clear that the cell-free layer after the constriction is enhanced as the constriction gets longer and narrower.

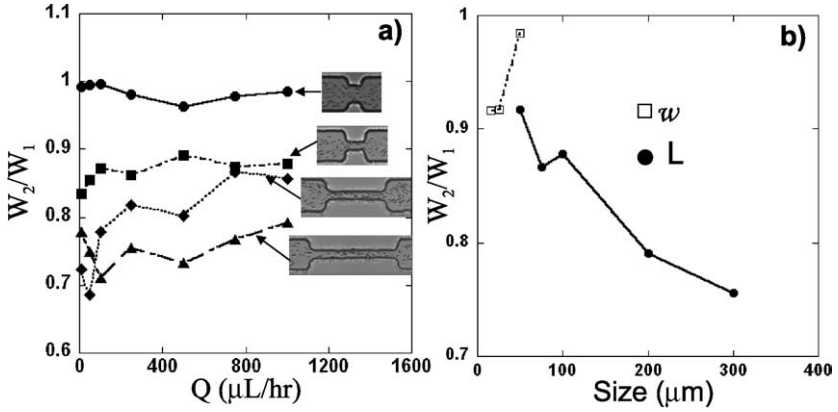

Fig. 4. (a) Ratio of the widths of distribution of the red blood cells W_2/W_1 versus the flow rate Q for different geometries of the constriction: • ($L = 50$ μm and $w = 50$ μm), ■ ($L = 75$ μm and $w = 25$ μm), ♦ ($L = 200$ μm and $w = 25$ μm) and ▲ ($L = 300$ μm and $w = 25$ μm). (b) Ratio of the widths of distribution of the cells, the mean value of W_2/W_1 extracted from Fig. 4a, versus the length L or the width w of the constriction. For both (a) and (b) the dextran solution has viscosity 0.02 Pa.s and the hematocrit concentration is 2.6%. Typical images of the relative length of the constriction are shown on Fig. 4a.

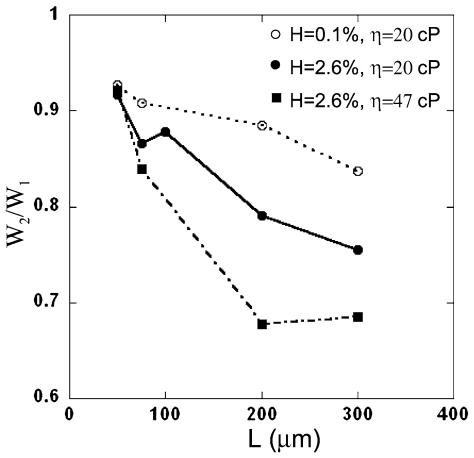

Fig. 5. Ratio of the widths of distribution of the cells W_2/W_1 versus the length L of the constriction (for $w = 25$ μm) for different hematocrit concentrations and solution viscosities.

There are several physical properties of the liquid and the cells that may impact the enhancement produced by the constriction so we next turn to these experiments. First, we modify the cell concentration (hematocrit). In Fig. 5, we report the ratio W_2/W_1 versus the length L of the constriction for the two different concentrations of 0.1% and 2.6% for a fixed outer fluid viscosity (0.02 Pa.s). The results illustrate that an increase in the cell concentration results in an enhancement of the width of the cell-free layer downstream.

We have modified the viscosity of the suspending fluid by changing the concentration of dextran. The results are presented in Fig. 5 for two different viscosities of the suspending fluid. An increase of about a factor two in the viscosity of the solution results in an enhancement in the thickness of the downstream cell-free layer.

We have already indicated that the deformability of the red blood cells is the key to understand the enhancement of the cell-free layer. Thus, we next report results for different degrees of deformability. Four types of particles are used to conduct the experiments: solid spherical beads, healthy cells, hardened red blood cells and hypotonic erythrocytes (i.e. cells that are swollen due to a lower osmotic pressure). For these experiments the viscosity of the suspending fluid is fixed at 0.02 Pa.s. The results are reported in Fig. 6 in two ways: in Fig. 6a we report W_2/W_1 as a function of the constriction length L for each of the different particles and in Figs 6b–d we report trajectories for each of the three different types of experiments with the red blood cells. We observe that the experiments conducted with rigidified red blood cells show an enhanced cell-free layer after the constriction compared to the cell-free layer upstream. However this effect is smaller than for healthy cells. The results in Fig. 6a indicate that an increase in the volume of the cells (i.e. the hypotonic data) leads to an enhancement of the downstream cell free-layer; see also the trajectories in Figs 6c,d.

3.3. Non-uniform cell concentration

The radial dispersion of solid and deformable objects in low-Reynolds-number flows is documented in the literature [9,10,13,16], but to the best of our knowledge the effect of a constriction on this dispersion has not been investigated. We previously noted in Fig. 3b that there was evidence pointing to the constriction giving rise to a local maximum in the cell number density at positions off the centerline.

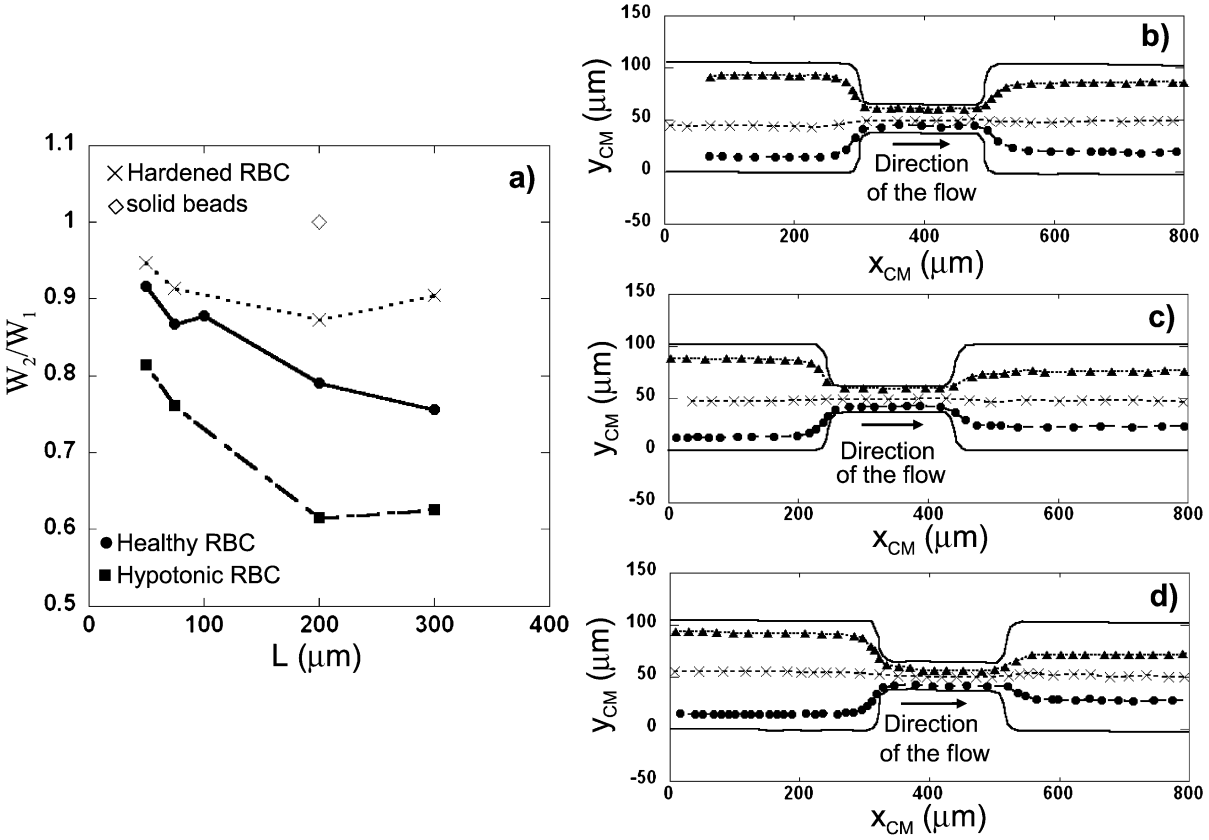

Fig. 6. (a) Ratio of the widths of distribution of the cells W_2/W_1 versus the length L of the constriction (for $w = 25$ μm) for different kind of red blood cells. Typical trajectories of (b) Hardened RBCs, (c) Healthy RBCs and (d) Hypotonic RBCs. The flow rate and the outer fluid viscosity are fixed respectively at $Q = 50$ μl/hr and $\eta = 0.02$ Pa.s.

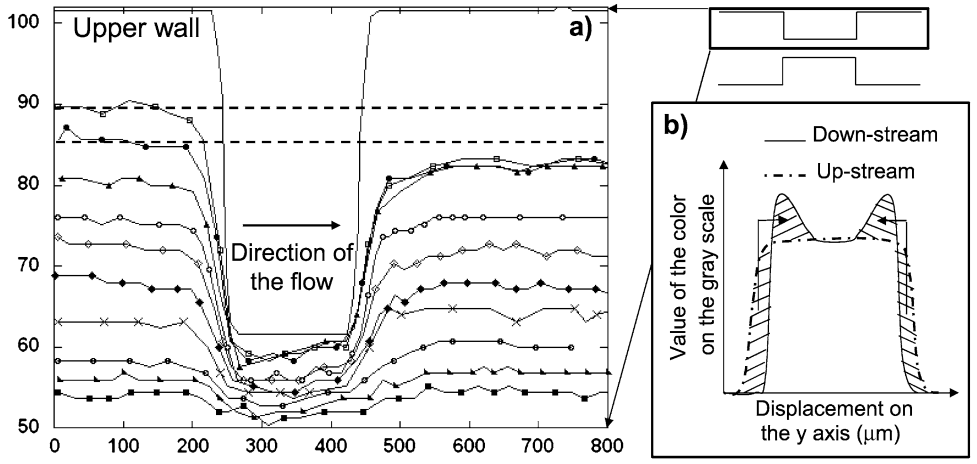

Fig. 7. (a) Trajectories of the center of mass of healthy cells dispersed in a suspending media with a viscosity of 0.02 Pa.s, $Q = 50$ μl/hr. (b) Sketch of the value of the intensity of the gray scale (or number density of cells) versus the displacement y across the channel: dashed line before and solid line after the constriction.

Therefore, we tracked individual cells in order to understand how the drift occurs at different positions across the channel; these results are shown in Fig. 7a. After the constriction, the three closest cells from the wall end up on about the same streamline. We also note that beyond a certain distance from the wall all of the cells have fore-aft symmetric trajectories.

These results provide a rational explanation for a local non-centered maximum in the number density of cells downstream of the constriction (see Fig. 3b) and the idea is indicated in the sketch in Fig. 7b: the concentration of cells gets modified by the migration across streamlines of the cells closest to the wall. Therefore, downstream of the constriction the maximum concentration is positioned just at the edge of the cell-free layer, while the cell concentration at the center of the channel remains unchanged.

4. Discussion

It is well known that flows in the microcirculation are characterized by a narrow cell-free layer adjacent to the walls of the capillaries. This cell-free layer is the origin of the Fåhraeus effect [11,18,20], which we observe upstream of the constriction. Moreover, we have identified a new feature of this old phenomenon, at least with respect to the interpretation in terms of the number density distribution of cells, through the enhancement of this cell-free layer downstream of a constriction. In order to understand the various results, we collect the major experimental observations in Table 1. In particular, the cell-free layer downstream is enhanced with increases in the length of the constriction, the concentration of cells, the viscosity of the suspending media, the cell deformability, and the volume of the cells. A decrease in the width of the constriction increases the cell-free layer. In addition, the flow rate does not affect in a significant way the measured downstream cell-free layer.

We interpret these results quantitatively in terms of the cross-streamline drift undergone by the cells [4,13,15,17], which occurs in the high shear rate region (i.e. the constriction). Although the detailed hydrodynamic description is complicated, some basic features are summarized in a model of a tank-treading ellipsoidal cell in a shear flow adjacent to a planar boundary [17]: the flow is assumed to be at low Reynolds numbers, and the object, assumed far from the wall, migrates away from the wall with a drift velocity v_d that depends approximately linearly on the shear rate $\dot{\gamma}$; the drift across streamlines results in enhancement of the cell-free layer. In our experiments, the cell experiences this drift primarily during the time τ it is in the constriction, since it is there that the shear rates are the highest. Although in our system we cannot expect quantitative agreement since the cells are never far from the wall, we use

Table 1
Summary of the effects of the different parameters on the cell-free layer downstream of the constriction

Parameters	Range of variation	Downstream cell-free layer
$Q \nearrow$	10–1000 μl/hr	weak effect
$L \nearrow$	50–300 μm	increased
$w \searrow$	50–15 μm	increased
hematocrit $\nearrow$	0.1–2.6%	increased
$\eta \nearrow$	20–47 cP	increased
deformability and volume $\nearrow$	solid beads, hardened, healthy and hypotonic cells	increased

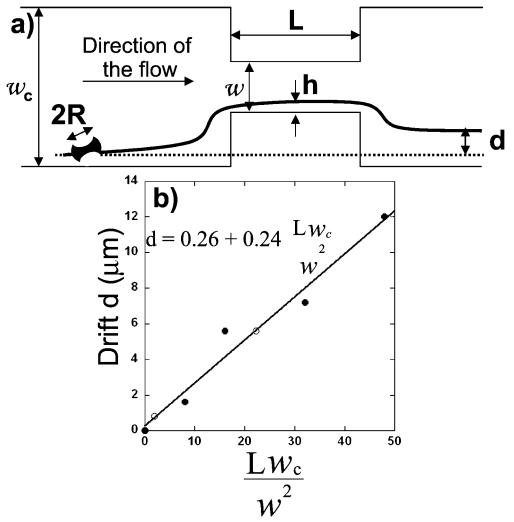

Fig. 8. (a) Definition of the parameters for the calculation of the drift d. (b) Drift measured (for $h = 2.4$ μm) versus Lw_c/w^2 for • $w = 25$ μm, L varying and for ∘ $L = 50$ μm, w varying. The suspending media has a viscosity of 0.02 Pa.s, and $Q = 50$ μl/hr.

the functional form suggested by Olla [17] as representative since the basic physical ideas are similar. The drift d is predicted to be of the form

$$d = v_d \cdot \tau, \tag{1}$$

with the drift velocity given by [16]

$$v_d = \kappa \frac{\dot{\gamma} R^3}{h^2}, \tag{2}$$

where R is the radius of the sphere of same volume as the cell, h is the distance of the particle to the wall in the constriction as described in Fig. 8a, and κ is a dimensionless parameter dependent on the orientation of the tank-treading cell and its shape, which in turns also depends on the viscosity ratio η_{in}/η_{out} between the cell and the suspending medium. The same scaling for the drift velocity was obtained by Chaffey et al. for the drift away from a wall of a deformable drop in a shear flow [4], in which case the parameter κ is proportional to the capillary number of the drop. Knowing the relationship between the shear rate and the flow rate Q for a rectangular channel of length L, width w and height H, estimating the passage time in the constriction as $\tau \approx LwH/Q$, and combining Eqs (1) and (2) we obtain (the known analytical result for flow in a narrow channel with $w < H$ gives $Q = \dot{\gamma} H w^2/6$)

$$d \approx 6\kappa \frac{LR^3}{wh^2}. \tag{3}$$

Neglecting the impact of shear rate on the parameter κ, we note that according to Eq. (3) the drift is independent of the flow rate applied, which is in agreement with the results shown in Figs 3c and 4a. In order to test (3) we selected a value of h (measured at the middle of the constriction, see Fig. 8a), representative of typical cells at the outermost edge of the cell-free layer, and measured the cross-streamline

drift downstream of the constriction for various values of both L and w. Because of the expansion of the channel, the spacing of the streamlines changes downstream of the constriction by the geometric ratio w_c/w, where w_c is the width of the main channel, and so for our measurement we expect $d \approx 6\kappa \frac{LR^3 w_c}{w^2 h^2}$. The experimental results are shown in Fig. 8b, which indicates that the final value of the cell-free layer d varies linearly with a parameter characteristic of the geometry of the constriction Lw_c/w^2 as predicted here.

It is possible to estimate the prefactors from the idealized theory of Olla [17] and also compare with the experimental measurements. We used the experimental value of $1/2$ for the ratio of the cell internal viscosity to the suspending fluid. We then used Eq. (3), modified by the factor w_c/w, to determine κ from the experimental data in Fig. 8b. We find $\kappa \approx 0.01$. For a deformed cell with a prolate shape with aspect ratio $1/5$ (consistent with the photographs) Olla's model calculation gives $\kappa \approx 0.45$. Thus, we conclude that qualitative and scaling features of the idealized theory are quite reasonable though quantitative agreement is clearly complicated owing to the complexity of the actual geometry and flow.

There are four further points to make. First, a decrease of the osmotic pressure of the suspending fluid from 300 to 200 mOsmol/kg results in a 23% increase of the volume of the cells [4]. In our experiments we find a significant enhancement of the cell-free layer when the cell volume is increased as documented on Fig. 6a. This result is quantitatively consistent with the dependence of d on the volume of the cell (R^3).

Second, when the concentration of the cells is increased, the effective viscosity of the solution is also increased [24], and, correspondingly, the parameter κ is known to decrease as the viscosity ratio between the cell and the suspending fluid decreases. This response is consistent with our experimental results relating the cell concentration and the viscosity of the suspending media.

Third, we recognize that the cell conditions we use are not physiological. First, we use low hematocrit in order to visualize single cells easily. Second, we use high buffer viscosity to avoid sedimentation of the cells in the feeding tubes of the microfluidic device. Third, as we show (contrast Figs 1b and 9 below) the basic response is similar for both the dilute and higher conditions. Indeed, in the last experiment in which we separate plasma from a blood solution, we use a concentration of 16% hematocrit, which is still smaller than the *in vivo* conditions, and we observe significant drift of cells away from the walls.

Fourth, we note that from a technological perspective, small devices introduced into a blood vessel in order to monitor, detect, and sample a flow, or to assist in drug delivery, may also act as a local obstruction. The results reported here suggest that downstream of such obstructions we might expect enhanced cell-free layers, which could impact transport processes in the circulation.

Finally, we apply the principle of the enhanced cell-free layer to the implementation of a microfluidic component for the separation of blood from plasma. For these experiments we used a 16% hematocrit and a flow rate $Q = 200$ μl/hr. In Fig. 9, we show a device where downstream of the constriction there are three channels in parallel. Because of the enhanced cell-free layer, the liquid collected in the outermost channels is totally composed of plasma (Fig. 9a). When we increase the width of the outermost channels to extract more plasma some cells are also entrained (Fig. 9b). In such cases, decreasing the width or increasing the length of the constriction again leads to the extraction of essentially pure plasma as shown successively in Figs 9c,d.

In addition, the volume of plasma withdrawn from the initial solution of blood can be estimated. Knowing the initial concentration of the solution (16 %v/v), its total volume (1 ml), the flow rate of injection (200 μl/hr), and estimating the flow rate through the outermost channels (typical particle mean velocities are measured to be about 1.4 mm/s), we can estimate the ratio between the initial volume of blood and the volume of plasma extracted. We find for the conditions shown in Fig. 9a that 24% of the

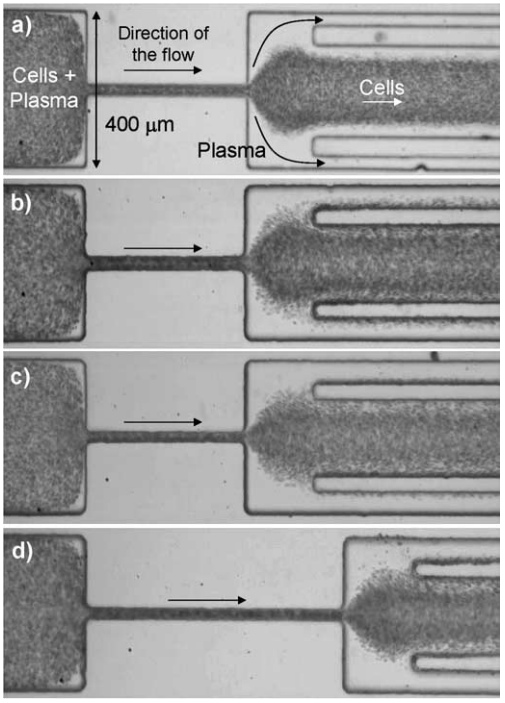

Fig. 9. A microfluidic design for separating plasma from blood. (a) $w = 25$ μm, $L = 500$ μm, $Q = 200$ μl/hr, width of the outermost channel is 30 μm. (b) Increase of the width of the outermost channel to 50 μm, with $w = 25$ μm, $L = 500$ μm, $Q = 200$ μl/hr. (c) Decrease of the constriction width to $w = 15$ μm with $L = 500$ μm, $Q = 200$ μl/hr and the width of the outermost channel is 50 μm. (d) Increase the length of the construction to $L = 800$ μm with $w = 25$ μm, $Q = 200$ μl/hr, and the width of the outermost channel is 50 μm.

initial plasma is continuously withdrawn, and, equivalently, the cellular content in the middle channel is enriched by 24%.

5. Conclusion

In this paper, we reported experiments on the flow of red blood cells in model constrictions. We showed how a rapid variation of the cross-section coupled with the deformability of the cells can produce a dramatic enhancement of the cell-free layer downstream of the constriction. We studied the influence of all the physical parameters on this geometrically enhanced cell-free layer. We used this knowledge to design a separator of blood plasma and demonstrated our control on the flow by varying the geometrical parameters such as the length and width of the constriction.

Finally, we note that such kinds of constrictions could mimic natural geometric blockages associated with a thrombotic microangiopathy and other diseases of the arterioles and venules [7]. Our *in vitro* experiment suggests that the cell-free layer present in the microcirculation could be affected by a natural or artificial constrictions, which we refer to a geometrically enhanced Fåhraeus effect. Other variants of these physical ideas to effect separation of plasma from blood cells should be possible as we have demonstrated in Fig. 9.

Acknowledgements

We thank the Harvard MRSEC for support of this research (DMR-0213805) and acknowledge Brian White for preliminary experiments on these systems.

References

[1] J.H. Barbee and G.R. Cokelet, Fåhraeus effect, *Microvasc. Res.* **3** (1971), 6–16.
[2] D.J. Beebe, G.A. Mensing and G.M. Walker, Physics and applications of microfluidics in biology, *Annu. Rev. Biomed. Eng.* **4** (2002), 261–286.
[3] H. Brenner and P.M. Bungay, Rigid-particle and liquid-droplet models of red cell motion in capillary tubes, *Fed. Proc.* **30** (1971), 1565–1576.
[4] C.E. Chaffey, H. Brenner and S.G. Mason, Particle motions in sheared suspensions VIII: Wall migration (theoretical), *Rheol. Acta* **4** (1965), 64; Correction **6** (1967), 100.
[5] A. Drochon, Rheology of dilute suspensions of red blood cells: experimental and theoretical approaches, *Eur. Phys. J. AP* **22** (2003), 155–162.
[6] D.C. Duffy, J.C. McDonald, O.J.A. Schueller and G.M. Whitesides, Rapid prototyping of microfluidic systems in poly(dimethylsiloxane), *Anal. Chem.* **70**(23) (1998), 4974–4984.
[7] E. Evans and Y.C. Fung, Improved measurements of erythrocyte geometry, *Microvasc. Res.* **4** (1972), 335–347.
[8] T.M. Fischer, M. Stöhr-Liesen and H. Schmid-Schönbein, Red-cell as a fluid droplet: Tank tread-like motion of the human erythrocyte membrane in shear flow, *Science* **202** (1978), 894–896.
[9] H.L. Goldsmith, Microscopic flow properties of red cells, *Fed. Proc.* **26** (1967), 1813–1819.
[10] H.L. Goldsmith, Red cell motions and wall interactions in tube flow, *Fed. Proc.* **30** (1971), 1578–1588.
[11] H.L. Goldsmith, G.R. Cokelet and P. Gaehtgens, Robin Fåhraeus – Evolution of his concepts in cardiovascular physiology, *Am. J. Physiol.* **257** (*Heart Circ. Physiol.* **26**), (1989), H1005–H1015.
[12] H.L. Goldsmith and J. Marlow, Flow behavior of erythrocytes. 1. Rotation and Deformation in dilute suspension, *Proc. R. Soc. Lond. B.* **182** (1972), 351–384.
[13] H.L. Goldsmith and S.G. Mason, Flow of suspensions through tubes. 2. Single large bubbles, *J. Colloid Sci.* **17** (1967), 448–476.
[14] Image J website, Z-project, Average intensity, http://rsb.info.nih.gov/ij/docs/menus/image.html#stacks/.
[15] A. Karnis, H.L. Goldsmith and S.G. Mason, Axial migration of particles in Poiseuille flow, *Nature* **200** (1963), 159–160.
[16] C.J. Koh, P. Hookham and L.G. Leal, An experimental investigation of concentrated suspension flows in a rectangular channel, *J. Fluid Mech.* **266** (1994), 1–32.
[17] P. Olla, The lift on a tank-treading ellipsoidal cell in a shear flow, *J. Phys. France II* **7** (1997), 1533–1540.
[18] A.R. Pries and T.W. Secomb, Rheology of the microcirculation, *Cardiovasc. Res.* **29** (2003), 143–148.
[19] A.R. Pries, K. Ley and P. Gaehtgens, Generalization of the Fåhraeus principle for microvessel networks, *Am. J. Physiol.* **251** (*Heart Circ. Physiol.* **20**) (1986), H1324–H1332.
[20] A.R. Pries, T.W. Secomb and P. Gaehtgens, Biophysical aspects of blood flow in the microvasculature, *Cardiovasc. Res.* **32** (1996), 654–667.
[21] S. Proske, B. Vollmar and M.D. Menger, Microvascular consequences of thrombosis in small venules: An in vivo microscopic study using a novel model in the ear of the hairless mouse, *Thrombosis Res.* **98** (2000), 491–498.
[22] S.S. Shevkoplyas, S.C. Gifford, T. Yoshida and M.W. Bitensky, Prototype of an in vitro model of the microcirculation, *Microvasc. Res.* **65** (2003), 132–136.
[23] S.S. Shevkoplyas, T. Yoshida, L.L. Munn and M.W. Bitensky, Biomimetic autoseparation of leukocytes from whole blood in a microfluidic device, *Anal. Chem.* **77** (2005), 933–937.
[24] T. Shiga, N. Meada and K. Kon, Erythrocyte rheology, *Critical Reviews in Oncology/Hematology* **10** (1990), 9–48.
[25] L. Thadikkaran, M.A. Siegenthaler, D. Crettaz, P.A. Queloz, P. Schneider and J.D. Tissot, Recent advances in blood-related proteomics, *Proteomics* **5** (2005), 3019–3034.